

Generalized Thermodynamics of Phase Equilibria in Scalar Active Matter

Supplemental Material

Alexandre P. Solon,¹ Joakim Stenhammar,² Michael E. Cates,³ Yariv Kafri,⁴ and Julien Tailleur⁵

¹*Massachusetts Institute of Technology, Department of Physics, Cambridge, Massachusetts 02139, USA*

²*Division of Physical Chemistry, Lund University, 221 00 Lund, Sweden*

³*DAMTP, Centre for Mathematical Sciences, University of Cambridge, Cambridge CB3 0WA, United Kingdom*

⁴*Department of Physics, Technion, Haifa, 32000, Israel*

⁵*Université Paris Diderot, Sorbonne Paris Cité, MSC, UMR 7057 CNRS, 75205 Paris, France*

(Dated: January 23, 2018)

References to equations or figures found in this Supplemental Material are labeled as S1, S2, etc. Other references correspond to figures and equations in the main text.

HYDRODYNAMICS OF QSAPS

In this section we derive the hydrodynamic equations of QSAPs interacting via a density-dependent velocity. The speed of particle i is given by $v[\tilde{\rho}(\mathbf{r}_i)]$ where

$$\tilde{\rho}(\mathbf{r}) = \int d\mathbf{r}' K(\mathbf{r}') \hat{\rho}(\mathbf{r} - \mathbf{r}') \quad (\text{S1})$$

with $K(\mathbf{r})$ an isotropic coarse-graining kernel, and $\hat{\rho}(\mathbf{r}) = \sum_j \delta(\mathbf{r} - \mathbf{r}_j)$ the microscopic particle density. For a system of size L , the (diffusive) relaxation time τ_D of the density profile scales as L^2 and is much larger than the microscopic orientational persistence time $\tau = (\alpha + (d-1)D_r)^{-1}$. To construct the large-scale dynamics of QSAPs, we first coarse-grain their dynamics on time scales such that $\tau \ll t \ll \tau_D \sim L^2$, following the method detailed in [1, 2]. In practice, we first construct a diffusive approximation to the dynamics of QSAPs on a time scale over which their density field does not relax so that the propulsion velocity of a single particle depends on its position and orientation through a function $v(\mathbf{r}_i)$ which is constant in time. Let us denote $\varphi(\mathbf{r})$ the probability density of finding a particle at position \mathbf{r} . Using the methods laid out in [2] leads, at the diffusion-drift level, to the Fokker-Planck equation

$$\dot{\varphi} = -\nabla \cdot [\mathbf{V}\varphi - D\nabla\varphi] \quad (\text{S2})$$

with

$$\mathbf{V} = -\frac{\tau v \nabla v}{d}; \quad D = D_t + \frac{\tau v^2}{d} \quad (\text{S3})$$

The Fokker-Planck equation (S2) for φ is equivalent to an Itô-Langevin dynamics for the position of the QSAP. From there, one can derive the collective dynamics of N QSAPs using Itô calculus [2–4]. For simplicity, we consider here the case $D_t = 0$. One then finds the coarse-

grained N -body density of QSAPs to follow the stochastic dynamics

$$\dot{\rho} = \nabla \cdot \left[\rho D(\tilde{\rho}) \nabla [\log \rho v(\tilde{\rho})] + \sqrt{2\rho D(\tilde{\rho})} \boldsymbol{\eta} \right], \quad (\text{S4})$$

We can now expand $\tilde{\rho}(\mathbf{r})$ in gradients of the density field

$$\tilde{\rho} \simeq \rho + \frac{1}{2} \ell^2 \Delta \rho + \mathcal{O}(\nabla^3) \quad (\text{S5})$$

with $\ell^2 = \frac{1}{2} \int r^2 K(\mathbf{r}) d\mathbf{r}$. In turn, this implies for the propulsion speed

$$v[\tilde{\rho}(\mathbf{r})] \approx v(\rho) + \ell^2 v'(\rho) \Delta \rho + \mathcal{O}(\nabla^3) \quad (\text{S6})$$

Finally one finds the self-consistent dynamics for ρ :

$$\dot{\rho} = \nabla \cdot \left[\rho D(\tilde{\rho}) \nabla \left(\frac{\delta \mathcal{F}}{\delta \rho} - \kappa(\rho) \Delta \rho \right) + \sqrt{2\rho D(\tilde{\rho})} \boldsymbol{\eta} \right], \quad (\text{S7})$$

where $\mathcal{F}[\rho] = \int d\mathbf{r} f[\rho(\mathbf{r})]$ and

$$f'(\rho) = \log[\rho v(\rho)]; \quad \kappa(\rho) = -\ell^2 \frac{v'(\rho)}{v(\rho)} \quad (\text{S8})$$

As hinted before [2, 4, 5], the non-locality of the density sampling results in a ‘surface tension generating’ term $\kappa(\rho)$.

Simulations

We conducted simulations of QSAPs in 1d on lattice and in a 2d continuous space. In the former case, particle i has a direction of motion $u_i = \pm 1$ which is randomized at rate α . It then jumps on the lattice site in direction u_i with rate $v[\tilde{\rho}(x_i)]$. In 2d off-lattice simulations, the dynamics of particle i at position \mathbf{r}_i and with orientation $\mathbf{u}_i = (\cos \theta_i, \sin \theta_i)$ is given by the Langevin equations

$$\begin{aligned} \dot{\mathbf{r}}_i &= v[\tilde{\rho}(\mathbf{r}_i)] \mathbf{u}_i + \sqrt{2D_t} \boldsymbol{\eta} \\ \dot{\theta}_i &= \sqrt{2D_r} \xi \end{aligned} \quad (\text{S9})$$

where $\boldsymbol{\eta}$ and ξ are delta-correlated Gaussian white noises of appropriate dimensionality. In addition to the continuous angular diffusion of Eq. (S9), the direction of motion

is randomized at discrete time events distributed exponentially in time with rate α .

In both types of simulations, the density $\bar{\rho}$ was computed according to Eq. (S1) (or its discretized version on lattice) with a bell-shaped kernel

$$K(r) = \frac{\Theta(r_0 - r)}{Z} \exp\left(-\frac{1}{1 - (\frac{r}{r_0})^2}\right) \quad (\text{S10})$$

with an interaction radius $r_0 = 1$ and normalization constant Z .

PFAPS

Model

All PFAP simulations were carried out in 2 dimensions using the isotropic Weeks-Chandler-Andersen pair potential:

$$V(r) = \left[4\epsilon\left(\left(\frac{\sigma}{r}\right)^{12} - \left(\frac{\sigma}{r}\right)^6\right) + \epsilon\right]\Theta(r_0 - r) \quad (\text{S11})$$

where σ controls the particle diameter through the cut-off imposed by the Heaviside function at $r_0 = 2^{1/6}\sigma$, ϵ controls the energy scale and r is the center-to-center separation between two particles. The dynamics of a particle is given by the Langevin equations:

$$\begin{aligned} \dot{\mathbf{r}}_i &= -\nabla_i V(r) + v_0 \mathbf{u}_i + \sqrt{2D_t} \boldsymbol{\xi}_i, \\ \dot{\theta}_i &= \sqrt{2D_r} \eta_i, \end{aligned} \quad (\text{S12})$$

where \mathbf{r}_i and θ_i are the position and orientation of particle i , v_0 is the self-propulsion speed, D_t and $D_r = 3D_t/\sigma^2$ are the translational and rotational diffusivities, and $\boldsymbol{\xi}_i$ and η_i are unit-variance, Gaussian white noises. A mobility μ in front of $\nabla_i V(\mathbf{r})$ has been chosen equal to one. All simulations were carried out using the molecular simulation package LAMMPS [6].

All simulation results are presented in units such that $\sigma = 1$ and $\epsilon = 1$. A time step of 5×10^{-5} was used throughout. As in [7], the Péclet number was varied by adjusting D_r (and accordingly D_t) while keeping the self-propulsion velocity constant at a value of $v_0 = 24$.

Simulations

Simulations were carried out in rectangular boxes of size $L_x \times L_y$ with periodic boundary conditions. We chose $L_x = L_y = 150$ for simulations in the single-phase region (Pe = 40 in Fig. 2a) and $L_x = 500$, $L_y = 300$, $N = 115,000$ particles for simulations at phase coexistence. In order to ensure a stable, flat (on average) interface spanning the $\hat{\mathbf{y}}$ -direction, these simulations were initiated by first equilibrating the particles in a smaller

box of size 300×300 with $v_0 = 0$, yielding a near-close-packed phase. After this initial equilibration, the box was expanded in the $\hat{\mathbf{x}}$ -direction and the activity was turned on, after which the system relaxed towards a phase-separated steady state. The simulations were run for a time $t = 1000$, the data being collected over the second half of this time.

We compute binodal densities by coarse-graining the local density on a grid using a weighting function $w(r) \propto \exp[-r_{\text{cut}}^2/(r_{\text{cut}}^2 - r^2)]$, where r is the distance between the particle and a grid point, and r_{cut} is a cut-off distance which was taken to be slightly larger than the grid spacing. Histograms of the density then show two peaks that we identify as the coexisting densities.

Construction of the equation of state

The total mechanical pressure of a bulk phase of PFAPs is composed of two terms: the *swim pressure* $P_S = \frac{v_0^2}{2D_r}\rho + \frac{v_0}{D_r}I_2$ and the *direct pressure* P_D [8]. In order to accurately predict the binodal densities of PFAPs, we need to construct accurate predictions for these two contributions in the full range of Péclet numbers considered. Since we cannot maintain stable homogeneous phases at arbitrary densities for $\text{Pe} > \text{Pe}_c$, we construct the equation of state (EOS) for $\text{Pe} = 40 < \text{Pe}_c$, and extrapolate to higher Péclet numbers using scaling arguments.

The swim-pressure part of the EOS can be measured by using the (exact) expression of P_S in terms of the two-point correlations in I_2 . One then obtains a numerical measure of $P_S(\rho)$ in an homogeneous phase, which following Ref. [8] we write as

$$P_S = \frac{6\text{Pe}}{\sigma}v_{\text{eff}}(\rho)\rho, \quad (\text{S13})$$

where $v_{\text{eff}}(\rho)$ is an *effective*, density-dependent swim speed which accounts for the slowing down of particles due to collisions. As was shown before [8–10], $v_{\text{eff}}(\rho)$ is well approximated by a linearly decreasing function up to densities near close packing. However, this is less accurate at high densities which are crucial for our purpose of computing the binodal densities. We are thus led to refine our previous EOS for the swim pressure [8] by including a quadratic term in ρ as well as a tanh function which ensures a smooth transition to $v_{\text{eff}} \rightarrow 0$ as ρ approaches close packing:

$$v_{\text{eff}}(\rho) = \frac{v_0}{2} \left[(1 - s_1\rho + s_2\rho^2) (1 - \tanh[s_3(\rho - s_4)]) \right], \quad (\text{S14})$$

where $s_1 - s_4$ are fitting parameters.

To extrapolate to higher Pe, we use the assumption (see Ref. [8]) that $v_{\text{eff}}(\rho)$ is independent of Pe. Note that, since the Péclet number is varied by changing D_r

while keeping v_0 constant, this is equivalent to assuming that the two-point correlations in I_2 are independent of D_r . This scaling assumption would certainly not hold if v_0 had been varied due to the relatively soft interparticle potential, not even after taking the trivial dependence of $v_{\text{eff}}(\rho)$ on v_0 into account.

The direct part of the EOS was obtained by fitting the numerical measurement (which makes use of the standard virial relation for pairwise additive forces [11]) to the following function

$$P_D(\rho) = d_1 [\exp(d_2\rho) - 1] + d_3 [\exp(d_4\rho) - 1], \quad (\text{S15})$$

where $d_1 - d_4$ are fitting parameters. This term is then assumed to be independent of Pe , which is again a reasonable approximation as long as v_0 is kept constant.

The numerical values and the fits with Eq. (S14) and (S15) for $\text{Pe} = 40$ are shown in Fig. S1, where we also check that our scaling arguments hold by comparing with the numerical measurements at $\text{Pe} = 20$.

Construction of the binodals

To construct the binodals, we first measured numerically profiles of $\rho(x)$ and $g(x)$ (given by Eq. (12)) across the gas-liquid interface. The gradient contributions to g were then obtained by subtracting the bulk contribution using the analytical EOS $g_0(\rho)$ evaluated along the measured density profile $\rho(x)$, i.e., $g_{\text{int}} = g(x) - g_0(\rho(x))$. g_{int} was then multiplied by the numerical derivative of the measured volume per particle, $\partial_x(\nu(x)) = \partial_x(\rho^{-1}(x))$, to yield the integrand on the RHS of Eq. (13). The value of this integral quantifies the violation of the equal-area Maxwell construction.

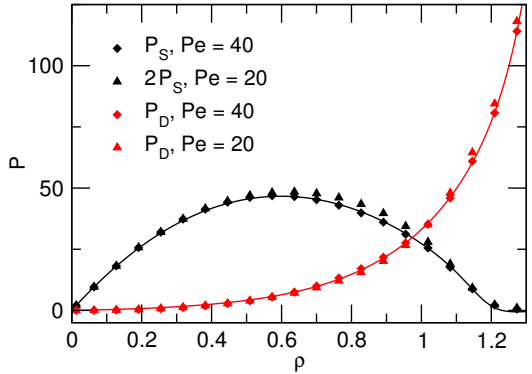


Figure S1. Values of P_S and P_D as a function of the average density ρ measured from simulations in the one-phase region $\text{Pe} < \text{Pe}_c$ (symbols). The solid lines show fits to the data at $\text{Pe} = 40$ using Eqs. (S13)–(S14) for P_S and Eq. (S15) for P_D . The data for P_S at $\text{Pe} = 20$ has been rescaled by a factor of 2 in accordance with our scaling assumption.

Finally, the value of \bar{g} on the LHS of Eq. (13) was adjusted such that the integral of $g_0(\nu) - \bar{g}$ between the intersects of \bar{g} and $g_0(\nu)$ equals the RHS integral. The associated values of ν_ℓ and ν_g are the predicted inverse coexistence densities, while the value of \bar{g} is the coexistence pressure.

- [1] M. Cates and J. Tailleur, *EPL (Europhysics Letters)* **101**, 20010 (2013).
- [2] A. Solon, M. Cates, and J. Tailleur, *The European Physical Journal Special Topics* **224**, 1231 (2015).
- [3] D. S. Dean, *Journal of Physics A: Mathematical and General* **29**, L613 (1996).
- [4] J. Tailleur and M. Cates, *Physical review letters* **100**, 218103 (2008).
- [5] R. Wittkowski, A. Tiribocchi, J. Stenhammar, R. J. Allen, D. Marenduzzo, and M. E. Cates, *Nature communications* **5** (2014).
- [6] S. Plimpton, *Journal of computational physics* **117**, 1 (1995).
- [7] J. Stenhammar, D. Marenduzzo, R. J. Allen, and M. E. Cates, *Soft Matter* **10**, 1489 (2014).
- [8] A. P. Solon, J. Stenhammar, R. Wittkowski, M. Kardar, Y. Kafri, M. E. Cates, and J. Tailleur, *Physical review letters* **114**, 198301 (2015).
- [9] Y. Fily and M. C. Marchetti, *Physical review letters* **108**, 235702 (2012).
- [10] J. Bialké, H. Löwen, and T. Speck, *EPL (Europhysics Letters)* **103**, 30008 (2013).
- [11] M. P. Allen and D. J. Tildesley, *Computer simulation of liquids* (Oxford university press, 1989).